Comparative analysis of upwelling influence between the western and northern coast of the Iberian Peninsula

I. Alvarez [a,b,*], M. Gomez-Gesteira [a], M. deCastro [a], M.N. Lorenzo [a], A.J.C. Crespo [a], J.M. Dias [b]

[a] EPhysLab (Environmental Physics Laboratory), Universidade de Vigo, Facultade de Ciencias, Ourense, Spain
[b] CESAM, Universidade de Aveiro, Departamento de Fisica, Aveiro, Portugal

ABSTRACT

Upwelling conditions have been simultaneously analyzed along the western and northern coast of the Iberian Peninsula in terms of wind forcing and water temperature response. The wind forcing analysis showed that the season under more upwelling favorable conditions corresponds to spring–summer (April–September) along the western coast and only to summer (June–August) along the northern one. Taking into account the upwelling period common to both coasts (June–August), it was observed that the occurrence of upwelling events simultaneously along both coasts is the most probable situation (∼46%) followed by upwelling unfavorable conditions also along both coasts (∼26%). The analysis of sea surface temperature data also showed the existence of an upwelling season in spring–summer along both coasts, although upwelling events are more frequent and intense along the western coast than along the northern one. Chlorophyll concentrations showed a high seasonal variability at the western coast with the highest concentrations values in spring–summer months while at the northern coast the maximum values were observed in spring and autumn.

© 2010 Elsevier Ltd. All rights reserved.

1. Introduction

Cape Finisterre marks an abrupt change in the coastline orientation of the northwestern coast of the Iberian Peninsula (IP) splitting this region in two different domains (Fig. 1): the Atlantic coast which lies in the N–S direction and the Cantabrian coast which lies in the W–E direction. These regions have an important hydrologic and biogeochemical activity, mainly attributable to coastal upwelling processes, and have been extensively studied during the last decades (Fraga, 1981; Botas et al., 1990; Borja et al., 1996, 2008; Bode et al., 2002). Several studies have been carried out in terms of wind-driven upwelling showing that the wind field is far from homogeneous in these areas and that wind observations at a single point, coastal or offshore, will not necessarily be representative of coastal conditions over a significant distance. In fact, some recent works carried out around the Galician coast (Torres et al., 2003; Gomez-Gesteira et al., 2006; Alvarez et al., 2008a) have shown that the upwelling frequency and intensity are influenced by the coastal orientation which modulates wind direction and intensity changing the upwelling favorable conditions prevalence at each coastal region. Coastal upwelling occurs mainly during the spring–summer months along the western and northern coast of the IP (Fraga, 1981; Botas et al., 1990; Borja et al., 1996, 2008; Lavin et al., 1998; Bode et al., 2002; Garcia-Soto et al., 2002; Llope et al., 2006; Alvarez et al., 2008b, 2010; Fontan et al., 2008). This upwelling generates an important primary production related to the presence of Eastern North Atlantic Central Water (ENACW, Fiuza, 1984; Ríos et al., 1992) near the coast, which can be upwelled inside the rias located in the region. Nevertheless, previous studies have shown that the mean long-term wind field's summer and winter patterns are not necessarily representative of particular years when summer-like upwelling patterns may also dominate in winter. Thus, wind patterns may alternate producing brief episodes of upwelling at the northern or western coast, or a combined pattern may occur producing weak upwelling on both coasts (Torres et al., 2003). In addition, along the western coast these upwelling events are more probable than along the northern one (Gomez-Gesteira et al., 2006; Alvarez et al., 2008a, 2008b) reaching probabilities around 60% and 30%, respectively, in summer. Although this coastal upwelling is basically a spring–summer process, it can also be observed in autumn–winter (Santos et al., 2001, 2004; Alvarez et al., 2003, 2009; Borges et al., 2003; deCastro et al., 2006, 2008a). This autumn–winter events can also be related to the presence of ENACW near coast (deCastro et al., 2006), although some authors have found different upwelled waters related to the Iberian Poleward Current (IPC, Frouin et al., 1990; Alvarez et al., 2003; Prego et al., 2007) and to shelf bottom seawater (Alvarez et al., 2009).

* Corresponding author at: EPhysLab (Environmental Physics Laboratory), Universidade de Vigo, Facultade de Ciencias, Ourense, Spain.
Tel.: +34 988 387 244; fax: +34 988 387 227.
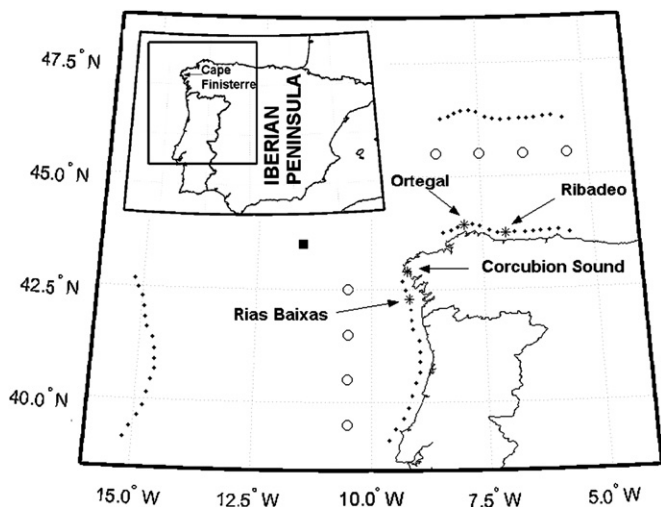*E-mail address:* ialvarez@uvigo.es (I. Alvarez).

Fig. 1. Map of the western and northern coast of the Iberian Peninsula. The black square and circles represent the points where Ekman transport data were considered. Black points represent the location where SST data were obtained. Asterisks represent the points where chlorophyll data were considered.

Most of the studies described above were mainly focused on the western or northern coast of the IP separately and therefore have different databases and temporal scales, making the comparison between both coasts more difficult.

The aim of the paper is a comparative analysis between upwelling features along the western and the northern coast of the Iberian Peninsula. The comparative analysis was carried out in terms of upwelling indices calculated from Ekman transport data (UI_{ET}). In addition, upwelling trends were also calculated along the northwestern coast from 1967 to 2008. The upwelling implications in the ecosystem were characterized by means of the sea surface temperature (UI_{SST}) and chlorophyll concentrations. Thus, wind-induced upwelling conditions and water response to this forcing will be analyzed simultaneously along both coasts.

2. Data and methods

Ekman transport data provided by the Pacific Fisheries Environmental Laboratory (PFEL) (http://www.pfeg.noaa.gov) were considered over the last 42 years (1967–2008). The PFEL distributes environmental index products and time-series data-bases to cooperating researchers, taking advantage of its long association with the U.S. Navy's Fleet Numerical Meteorology and Oceanography Centre (FNMOC). FNMOC produces operational forecasts of the state of the atmosphere and the ocean several times daily and maintains archives of several important para-meters. These parameters are model derived products which are routinely distributed to researchers. For our purposes six-hourly Ekman transport data model derived from Sea Level Pressure were considered at 4 points selected along the western coast of the IP (42.5°N, 41.5°N, 40.5°N, 39.5°N along 10.5°W) and 4 points selected along the northern one (8.5°W, 7.5°W, 6.5°W, 5.5°W along 45.5°N) (Fig. 1, circles) on an approximately 1° × 1° grid. A control point was also considered at 43.5°N, 11.5°W (Fig. 1, black square). These data sets were averaged to obtain daily series.

Upwelling Index from Ekman transport data (UI_{ET}) can be calculated as the transport component in the direction perpendicular to the shoreline (Bakun, 1973; Nykjaer and Van Camp, 1994; Gomez-Gesteira et al., 2006). Ekman transport components can be defined in terms of wind speed, W, the seawater density, $\rho_w = 1025$ kg m^{-3}, a dimensionless drag

coefficient, $C_d = 1.4 \times 10^{-3}$, and the air density, $\rho_a = 1.22$ kg m^{-3}, by means of

$$Q_x = \frac{\rho_a C_d}{\rho_w f}(W_x^2 + W_y^2)^{1/2} W_y \quad \text{and} \quad Q_y = -\frac{\rho_a C_d}{\rho_w f}(W_x^2 + W_y^2)^{1/2} W_x$$

f is the Coriolis parameter defined as twice the vertical component of the Earth's angular velocity, Ω, about the local vertical given by $f = 2\Omega \sin(\theta)$ at latitude θ. Finally, x subscript corresponds to the zonal component and the y subscript to the meridional one. Although the shoreline angle along the western and northern coast of the IP changes slightly from the northern to the southern limit and from the western to the eastern limit, macroscopically it can be considered approximately 90° and parallel to the equator, respectively. Thus, $-Q_x$ can be directly considered as the UI_{ET} along the western coast and Q_y along the northern one. Positive (negative) UI_{ET} values mean upwelling favorable (unfavorable) conditions.

The prevalence of upwelling favorable conditions can be characterized by the probability of finding consecutive days under these upwelling favorable conditions ($UI_{ET} > 16$ m^3 s^{-1} km^{-1}). Note that the threshold (16 m^3 s^{-1} km^{-1}) correspond to winds with intensity lower than 1 m s^{-1} to remove calms.

The real impact of upwelling events can be quantified by means of a new term defined as Upwelling Impact (U_{Imp}). This term can be calculated taking into account the upwelling intensity and the number of days under upwelling favorable conditions by means of the expression $U_{Imp} = \sum_{i=1}^{N} n_i \langle UI_{ET} \rangle_i^F / N_d$. n_i is the number of consecutive days under upwelling favorable conditions considering $n_i \geq 4$. In fact, previous studies around the north-western coast of the IP proved that upwelled water can be easily identified when upwelling favorable conditions persist for more than 3–4 days (Alvarez-Salgado et al., 2000, 2006; Alvarez et al., 2005). $\langle UI_{ET} \rangle_i^F$ is the mean intensity of UI_{ET} during these days, N is the number of events per year and N_d is the number of days of the period under study.

Weekly mean SST data was obtained from night time measurements carried out by the Advanced Very High Resolution Radiometer on board NOAA series satellites (http://poet.jpl.nasa.gov). Data are available since 1985 with a spatial resolution of 4 km. For each grid point, an SST value is computed as the average of all cloud-free multichannel measurements available for 1 week. Two discrete sets of points placed along the northwestern coast of the IP were generated (Fig. 1, black points). Along the western coast, 16 points were considered at 20 and 500 km from the coast and along the northern one, 16 points were placed at 20 and 300 km from the coast. The distance of the oceanic points from the northern coast has been considered lower in order to avoid the possible effects of the French coast. Discretization effects were smoothed by calculating the SST monthly values at each point as the average of its nearest neighbors in latitude or longitude, depending on coast orientation. The distance between adjacent points is approximately 20 km.

The SST Upwelling Index (UI_{SST}) can be calculated as the SST difference between coastal and oceanic points at the same latitude (western coast) or longitude (northern coast). Along the western coast of the IP the distance of the oceanic points has been considered taking into account that the general patterns of the spatio-temporal variability of the index are similar within the range 400–1000 km offshore (Nykjaer and Van Camp, 1994; Santos et al., 2005; deCastro et al., 2008b). Along the northern coast this difference cannot be considered as an absolute Upwelling Index since temperature also changes with latitude due to differences in solar heating. In order to compare the UI_{SST} calculated along both coasts of the IP, a previous analysis was carried out to characterize these temperature changes in latitude. Four control points were considered along 43.5°N and 46.5°N

from 11°W to 14°W with a distance between points of 1° in longitude. SST difference was calculated between each point at the same longitude and it was found that temperature values tends to decrease northward on the order of 0.30 °C latitude^{-1} at the 4 control points. Taking into account that the oceanic points along the northern coast of the IP are located approximately 3° northward to the coastal ones, it can be considered that the temperature difference between points due to changes in latitude is around 0.9 °C. Thus, the SST values obtained at the oceanic points can be corrected considering this value and then, the SST difference between coastal and oceanic points (UI_{SST}) can be calculated. Negative (positive) UI_{SST} values mean upwelling favorable (unfavorable) conditions.

The analysis of chlorophyll concentration was based on the data of the SeaWIFS radiometer. Data were obtained from NASA's Goddard Space Flight Center (http://oceancolor.gsfc.nasa.gov/SeaWiFS/) available for the period 1998–2007 with a spatial resolution of 9 km × 9 km and a temporal resolution of 8-days. Data were considered at 2 points selected along the western coast of Galicia (Corcubion Sound: 9.2°W, 42.9°N; Rias Baixas: 9.1°W, 42.3°N) and 2 points selected along the northern one (Ortegal: 7.9°W, 43.9°N; Ribadeo: 6.9°W, 43.7°N) (Fig. 1, asterisks). These control points were considered along the Galician coast due to the presence of the coastal systems forming the Galician Rias characterized by a great primary productivity which can supports an intense raft culture of mussels. In addition, the first point considered at the western coast (Corcubion Sound) has been selected in order to compare the obtained results with the recent work carried out by Varela et al. (2010). These authors also used the SeaWIFS database to analyze upwelling blooms at the Corcubion Sound, an open bay located in the NW of the Iberian Peninsula delimited by Cape Finisterre.

3. Results

3.1. Wind-induced upwelling conditions

3.1.1. Inter-annual variability

The temporal evolution of the UI_{ET} from 1967 to 2008 along the western and northern coast of the IP analyzed at the 4 control points located at each coast is shown in Fig. 2. The inter-annual evolution of UI_{ET} (Fig. 2(a, b)) shows that UI_{ET} values tend to be higher along the western coast than along the northern one throughout the whole period. Taking into account the small latitudinal and meridional changes observed in Fig. 2(a, b), an average of UI_{ET} can be calculated considering all the control points at each part of the coast. Fig. 2(c) shows the inter-annual evolution of the meridional average of UI_{ET} for the western coast and Fig. 2(d) shows the latitudinal average of UI_{ET} for the northern coast. Both signals present maxima in spring–summer and minima in autumn–winter showing important differences among years. In addition, along the western coast the signal tends to be displaced toward positive values and along the northern one the signal is displaced toward negative values.

The inter-annual variability observed along both coasts in Fig. 2 can also be analyzed by means of the monthly evolution of the spatially averaged UI_{ET}, taking into account each year from 1967 to 2008 (Fig. 3(a, b)). A 4-year running average was considered to smooth out the short term fluctuations. The season under more upwelling favorable conditions for each year along the western coast corresponds to spring–summer (April–September), while along the northern coast this period is shorter (June–August). In addition, during the upwelling season some changes in the UI_{ET} values throughout the whole time period can be observed. Along the western coast (Fig. 3(a)), it is possible to observe high UI_{ET} values

(~ 700 m^3 s^{-1} km^{-1}) at the end of the 1970s. UI_{ET} decreases from this date to the beginning of the 1990s when a new increasing period can be observed (maximum value ~ 800 m^3 s^{-1} km^{-1}), lasting until the end of this decade. Along the northern coast, the UI_{ET} behavior during the upwelling season is different showing lower values than the ones corresponding to the western coast, in accordance with Fig. 2. Small variations can be observed throughout the whole period as the slight UI_{ET} decrease observed at the middle of the 1970s and the one observed from the end of the 1990s until the end of the period.

The annual evolution of UI_{ET} calculated averaging monthly data from 1967 to 2008, shows the duration of the upwelling favorable conditions at both coasts (Fig. 4(a, b)). The pattern of this monthly average is also similar along both coasts, although there are some differences. Positive values of UI_{ET} (upwelling favorable conditions) are observed from March to September along the western coast but only from June to August along the northern one. This situation can be better observed considering the spatially averaged UI_{ET} at the western coast (Fig. 4(c)) and the northern one (Fig. 4(d)). The maximum value of UI_{ET} is observed in July at both coasts, although the highest values along the western coast are close to 700 m^3 s^{-1} km^{-1} and only close to 300 m^3 s^{-1} km^{-1} along the northern one. For the rest of the year UI_{ET} shows negative or practically null values. The error bars were calculated using the standard deviation of the monthly data, $\sigma(UI_{ET})$. Error bars are observed to be negligible compared to the amplitude of the annual cycle calculated at each coast.

3.1.2. Upwelling frequency

Daily UI_{ET} from 1967 to 2008 was analyzed at the control point 43.5°N, 11.5°W (Fig. 1, black square) during the upwelling season common to both coasts (June–August) to better compare the upwelling occurrence along the western and northern coast. Fig. 5 shows daily UI_{ET} calculated for the western ($UI_{ET(W)}$) and northern ($UI_{ET(N)}$) coast, separated in quadrants. Positive values of $UI_{ET(W)}$ and $UI_{ET(N)}$ (quadrant I) correspond to upwelling favorable conditions at both coasts showing that $\sim 46\%$ of data keep these conditions, being are more favorable at the western coast ($UI_{ET(N)}/UI_{ET(W)} = 0.83$). The percentage of data corresponding to upwelling unfavorable conditions at both coasts (quadrant III) is lower ($\sim 26\%$). Quadrant II corresponds to upwelling favorable conditions at the northern coast (positive $UI_{ET(N)}$) and upwelling unfavorable conditions at the western one (negative $UI_{ET(W)}$) showing that the probability of observing this situation is very low ($\sim 2\%$). Quadrant IV (negative $UI_{ET(N)}$, positive $UI_{ET(W)}$) corresponds to the opposite pattern observed in quadrant II with a higher probability ($\sim 26\%$) indicating that these conditions are more frequent. In addition, the linear fit at both quadrants (II, IV) presents specific values of $UI_{ET(N)}/UI_{ET(W)} = -0.60$ and $UI_{ET(N)}/UI_{ET(W)} = -0.75$ showing that UI_{ET} values are more important at the western coast. Upwelling events along the western and northern coast of the IP were also analyzed considering decadal periods. Table 1 shows the linear fit ($y = ax$) and the percentage of events obtained at each quadrant taking into account these different decadal periods. The most probable conditions can be observed at quadrant I for all decades corresponding to the situation of upwelling favorable conditions along both coasts, with values ranging from $\sim 55\%$ at the first decade (1967–1976) to $\sim 41\%$ at the last one (1997–2006). On the contrary, the less probable conditions correspond to quadrant II (positive $UI_{ET(N)}$, negative $UI_{ET(W)}$) with values between $\sim 1\%$ and 4%. Quadrants III and IV present similar probability values following the pattern observed for the whole time period (Fig. 5) with values ranging from 21% to 30%. With regard to the linear fit, it is possible to observe inter-decadal variations considering the same quadrant. For example, the situation corresponding to quadrant III (upwelling unfavorable conditions
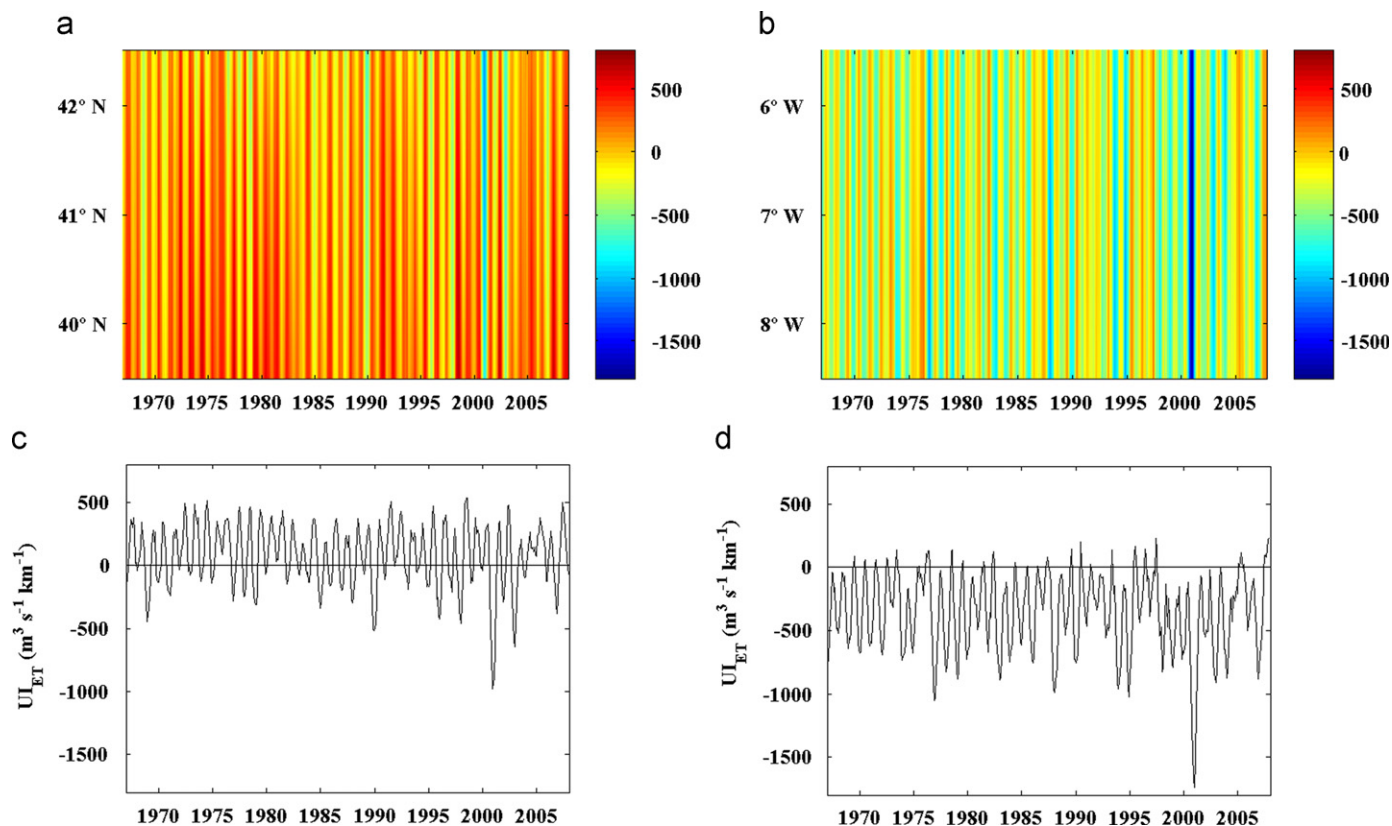
a

b

c

d

Fig. 2. Inter-annual evolution of UI_{ET} from 1967 to 2008 along the western (a) and northern (b) coast of the IP. Inter-annual evolution of the spatially averaged UI_{ET} from 1967 to 2008 along the western (c) and northern (d) coast of the IP.

along both coasts) during the second decade (1977–1986) shows a value of $UI_{ET(N)}/UI_{ET(W)}=1.00$ indicating that upwelling conditions are comparable at both coasts. During the third decade (1987–1996) UI_{ET} values are more important at the northern coast ($UI_{ET(N)}/UI_{ET(W)}=1.35$) and during the last one (1997–2006) upwelling unfavorable conditions are more significant at the western coast ($UI_{ET(N)}/UI_{ET(W)}=0.95$).

Upwelling occurrence can also be studied considering the mean number of days per month under upwelling favorable conditions ($UI_{ET}>16\ m^3\ s^{-1}\ km^{-1}$) from 1967 to 2008 at the control points. For the sake of clarity only the two control points located at the extreme part of each side of the IP coast were represented (Fig. 6(a)). Along the western coast the number of days increases from the northern (42.5°N) to the southern part (39.5°N). On the contrary, along the northern coast both control points show a similar number of days. The highest number of days under favorable conditions is observed during the spring–summer months at both coasts, with higher values along the western coast (20–28 days per month) than along the northern one (12–14 days per month). During autumn–winter the number of days under favorable conditions is lower at both coasts and, in addition, is also higher along the western coast (11–18 days per month) than along the northern one (8–10 days per month).

Upwelling prevalence during the upwelling season can be characterized by the probability of finding consecutive days under upwelling favorable conditions ($UI_{ET}>16\ m^3\ s^{-1}\ km^{-1}$). Taking into account the results obtained in previous figures, the upwelling duration was analyzed from April to September along the western coast and from June to August along the northern one (Fig. 6(b)). Along both coasts it is possible to observe how the upwelling probability decreases at all control points when the number of consecutive days under favorable conditions increases. In addition, probabilities are always lower along the northern

coast. At the western coast the upwelling probability increases southward in accordance with the previous figure, while at the northern coast, although the variation between points is practically negligible, it is possible to observe a slight decrease eastward. The highest probability values can be observed between 1 and 5 days at both coasts with values decreasing from around 70–80% to 50–60% at the western coast and from around 50% to 20% at the northern one.

3.1.3. Upwelling trends

The upwelling recurrence during the season under more upwelling favorable conditions was analyzed by means of the mean intensity of UI_{ET} and the variation in the number of days per year under favorable conditions for the period 1967–2008. For the sake of clarity, only one control point was considered at each coast (42.5°N western coast, 8.5°W northern coasts). A 2-year running average was considered for each point to better observe the overall behavior. At the western coast (Fig. 7(a)) upwelling intensity tends to increase throughout the whole period of time showing two maxima. The first one corresponds to the end of the 1970s and the second one to the end of the 1990s in accordance with the pattern shown in Fig. 3(a). At the northern coast (Fig. 7(b)) the amplitude range of UI_{ET} values varies slightly throughout the whole period, but 3 minima can be observed. The first one occurs at the middle of the 1970s, the second one at the middle of the 1980s and the third one at the end of the 1990s. Only the first and last minima were clearly observed in Fig. 3(b). General trends were analyzed by fitting these signals to a straight line. Thus, the upwelling intensity along both coasts shows a positive trend with values around $5\ m^3\ s^{-1}\ km^{-1}\ yr^{-1}$ at the western coast and around $1\ m^3\ s^{-1}\ km^{-1}\ yr^{-1}$ at the northern one ($p<0.01$).

The variation in the number of days under upwelling favorable conditions along the western coast (Fig. 7(c)) shows a repetitive
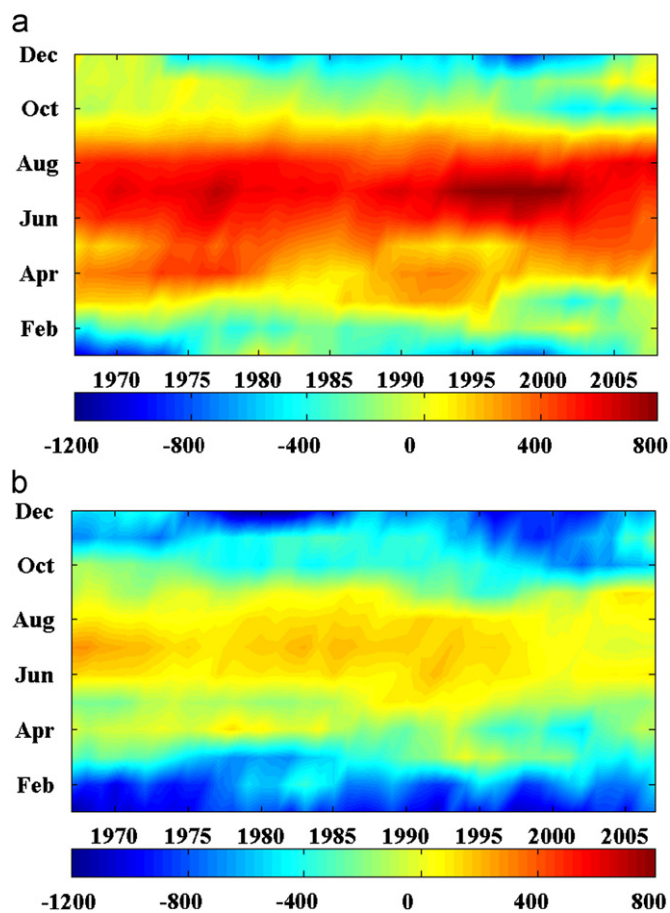
Fig. 3. Monthly evolution of the spatially averaged UI_{ET} from 1967 to 2008 along the western (a) and northern (b) coast of the IP.

dome-shaped pattern with decadal variations. Considering the whole time period (1967–2008), the number of days shows a negative trend with a value around -0.4 d yr^{-1} ($p < 0.01$). Along the northern coast (Fig. 7(d)), it is also possible to observe a negative trend with a value of -0.4 d yr^{-1} ($p < 0.01$).

In addition to the mean intensity of UI_{ET} and the variation in the number of days per year under favorable conditions, the Upwelling Impact (U_{Imp}) was also analyzed. At the western coast (Fig. 7(e)) the control point shows a slight positive trend, while at the northern one (Fig. 7(f)) the trend is negative with a low significance level ($p < 0.01$) at both coasts.

Trends for these variables were also analyzed at the 8 control points and represented in Table 2. The $\langle UI_{ET} \rangle^F$ along the western coast shows positive values at all points. The northern coast shows a different behavior with positive values at the 2 westernmost points and negative values for the 2 easternmost points. The variation in the number of days shows negative values at both coasts with higher ones at the western coast. In addition, at the northern coast values tend to increase eastward. The U_{Imp} along the western coast also shows positive values at all points decreasing southward, while at the northern coast values are negative with similar values at each point.

3.2. Implications of upwelling events

3.2.1. SST response to wind forcing

UI_{SST} was calculated taking into account the sea surface temperature difference between the coastal and oceanic points

at the same latitude at the western coast and at the same longitude at the northern one (Fig. 1, black points). Negative (positive) UI_{SST} values mean upwelling favorable (unfavorable) conditions. Fig. 8 shows the UI_{SST} temporal evolution from 1985 to 2008 along the western (Fig. 8(a, c)) and northern coast (Fig. 8(b, d)). The inter-annual evolution of the UI_{SST} presents an annual cycle along the western coast (Fig. 8(a)) with positive values in autumn–winter and negative values (upwelling favorable conditions) in spring–summer. Along the northern coast it is also possible to see this annual cycle although the temperature differences are lower than along the western coast. Considering the small spatial variations observed in these figures, the spatially averaged UI_{SST} can also be calculated at each part of the coast taking into account all control points (Fig. 8(c, d)). Both signals are irregular showing important differences among years with maximum UI_{SST} values in autumn–winter and minimum ones in spring–summer at both coasts. In addition, the signal tends to be displaced toward negative values at both coasts.

The annual cycle observed in the previous figure, can also be determined by the monthly average of the UI_{SST} at each coast (Fig. 9(a, b)). At the western coast UI_{SST} (Fig. 9(a)) shows positive values (upwelling unfavorable conditions) between January and May at the northern part of the coast (43–42°N). Southward (42–39°N) these positive values are observed only from March to April. For the rest of the year, UI_{SST} presents negative values showing the existence of a clear upwelling season between June and November with the strongest negative values observed in August–September. The behavior at the northern coast is similar with positive UI_{SST} values from January to April (Fig. 9(b)). From April to August UI_{SST} values are positive at the easternmost part of the coast (5.5–6.5°W) decreasing westward until reaching negative values at the westernmost point (8.5°W). For the rest of the year, UI_{SST} shows negative values with a minimum value observed in September–October at the western area. Considering the spatially averaged UI_{SST} along the western and northern coast is possible to analyze the global behavior of each coast (Fig. 9(c, d)). At the western coast negative values can be observed throughout the whole time period. From January to May UI_{SST} varies slightly with values ranging from -0.5 to 0 °C, while from June to December negative values increase showing a minimum (around -2.5 °C) in August–September. At the northern coast UI_{SST} also tends to be negative all over the year except from January to February when small positive values (0.2 °C) are observed. For the rest of the year values range from 0 to -0.5 °C showing that temperature differences between coastal and oceanic locations are lower than along the western coast. The minimum value is slightly displaced relating to the situation corresponding to the western coast and is observed in September–October. The error bars in Fig. 9(c, d) were calculated using the standard deviation of the monthly data, $\sigma(UI_{ET})$. Along the western coast error bars are observed to be negligible compared to the amplitude of the annual cycle, while at the northern one these values are similar to the amplitude range, especially from June to October.

3.2.2. Chlorophyll concentration

Variations of chlorophyll concentration were analyzed from monthly SeaWiFS data obtained from 1998 to 2007 at the control points shown in Fig. 1. A 2-month running average was considered for each point to better observe the overall behavior. The temporal variation of chlorophyll concentration along the western coast (Fig. 10(a)) shows an important inter-annual variability at both control points. The highest concentrations can be observed generally during the spring months in agreement with the known spring blooms which usually overlap with
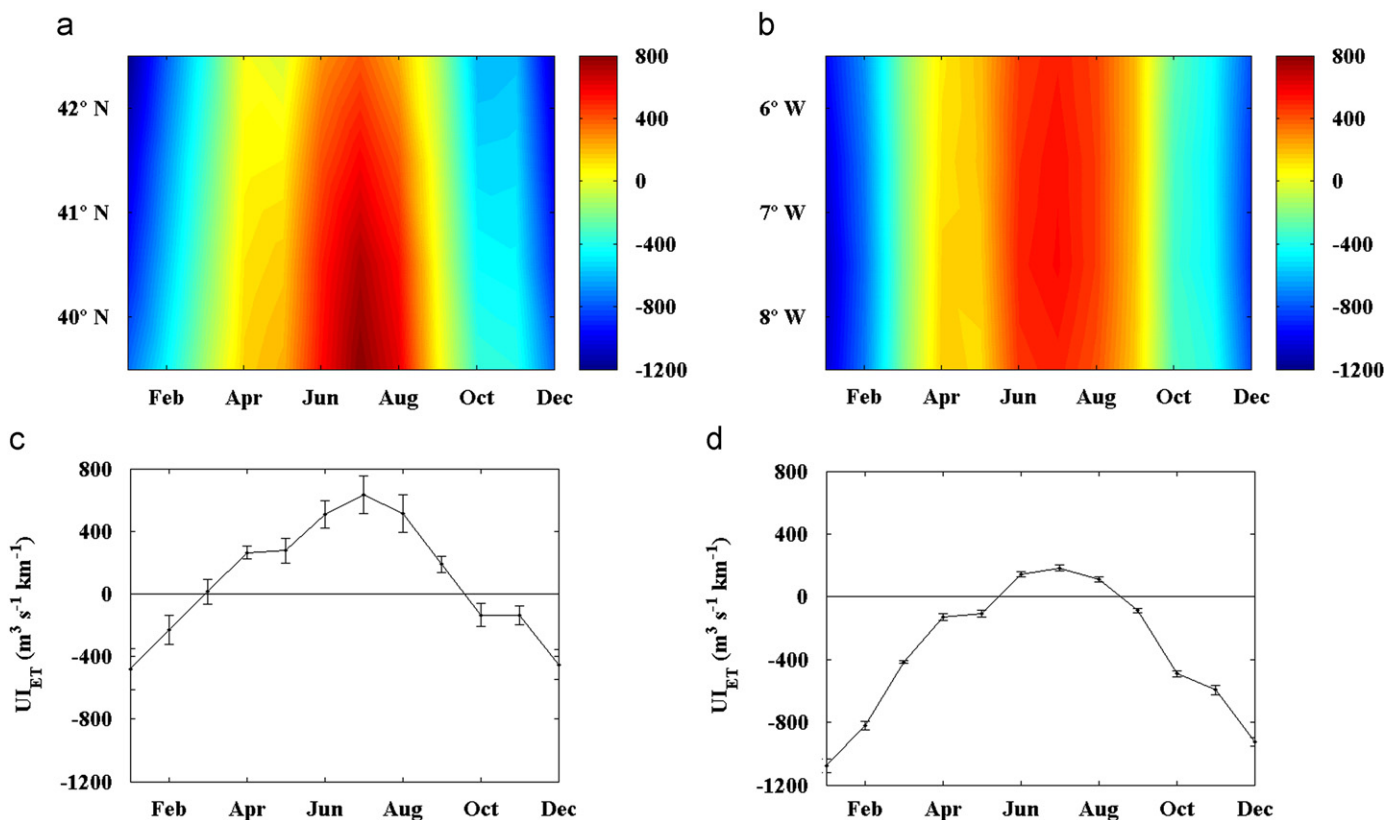
Fig. 4. Mean annual evolution of UI_{ET} from 1967 to 2008 along the western (a) and northern (b) coast of the IP. Annual cycle of UI_{ET} spatially averaged from 1967 to 2008 along the western (c) and northern (d) coast of the IP.
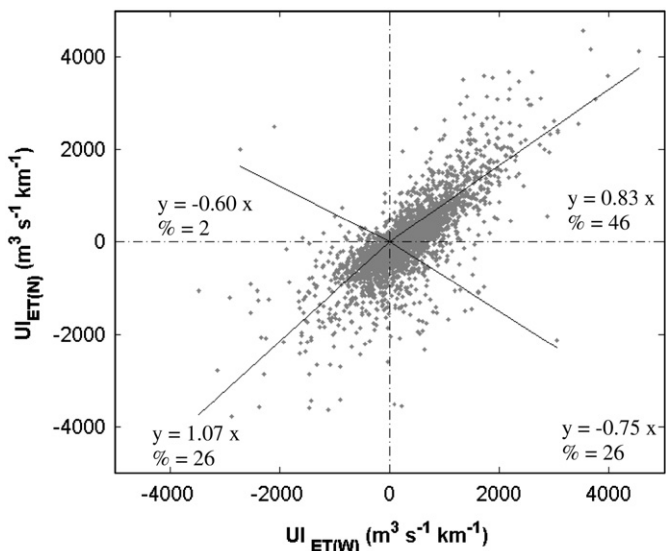

Fig. 5. Daily Upwelling Index under upwelling favorable conditions for the western ($UI_{ET(W)}$) and northern ($UI_{ET(N)}$) coast of the IP calculated at the control point 43.5°N, 11.5°W (Fig. 1, black square) from June to August over the period 1967–2008. Data are separated in quadrants, so positive values of $UI_{ET(W)}$ and $UI_{ET(N)}$ (quadrant I) correspond to upwelling favorable conditions at both coasts and negative values (quadrant III) correspond to unfavorable conditions. Straight lines show the linear fit ($y=ax$) at each quadrant ($p > 0.01$). The percentage (%) of total data found at each quadrant is also shown.

Table 1
Linear fit of daily upwelling index under upwelling favorable conditions for the western ($UI_{ET(W)}$)and northern ($UI_{ET(N)}$) coast ($y=ax$; $p > 0.01$), correlation coefficient and percentage of events obtained taking into account the whole period under study (1967–2008) and the different decadal periods from June to August. Data are separated in quadrants, so positive values of $UI_{ET(W)}$ and $UI_{ET(N)}$ (quadrant I) correspond to upwelling favorable conditions at both coasts and negative values (quadrant III) correspond to unfavorable conditions.

	Quadrant I			Quadrant II			Quadrant III			Quadrant IV		
	a	r	%	a	r	%	a	r	%	a	r	%
1967–2008	0.83	0.79	46	−0.60	0.66	2	1.07	0.47	26	−0.75	0.24	26
1967–1976	0.94	0.77	55	−0.47	0.58	3	1.17	0.49	21	−0.80	0.21	21
1977–1986	0.81	0.78	44	−0.31	0.36	4	1.00	0.23	27	−0.57	0.37	25
1987–1996	0.74	0.77	46	−1.12	0.80	1	1.35	0.56	23	−0.92	0.38	30
1997–2006	0.82	0.86	41	−0.54	0.74	3	0.95	0.58	29	−0.83	0.42	27

(Fig. 10(b)) the observed situation is different. Both control points show a similar pattern throughout the period with the highest concentration values during spring and autumn. Values are much lower than along the western coast although the chlorophyll concentration maxima (1–2 mg m^{-3}) can be also observed in 2005.

The annual variation of chlorophyll concentration was calculated from weekly data from 1998 to 2007. At the western coast (Fig. 10(c)), the southernmost point presents higher values all over the year with a fluctuating pattern. The maximum concentrations were observed in summer. At the northern coast (Fig. 10(d)), the variation of chlorophyll is of lower amplitude than along the western coast showing maxima in spring and autumn and minima in summer.
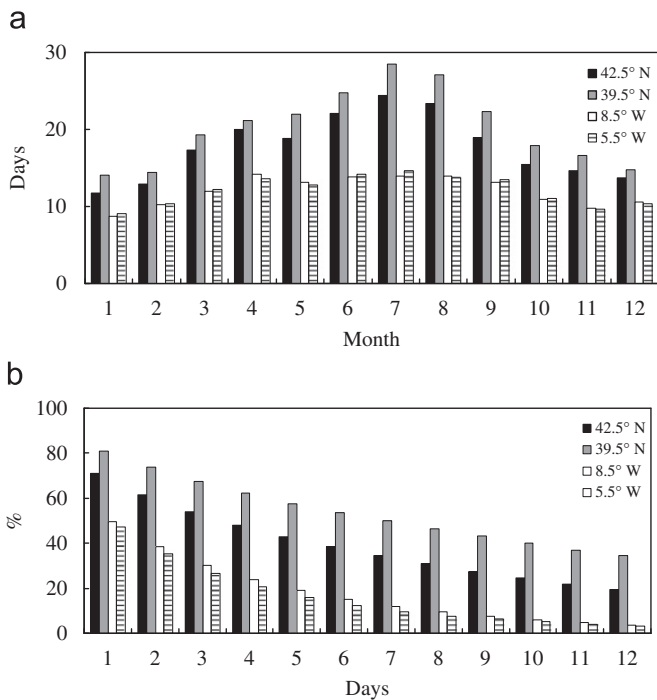
upwelling blooms from April to October. The chlorophyll concentration maxima (6–7 mg m^{-3}) occur in 2005 during summer. At the control points located along the northern coast

a

b

Fig. 6. (a) Number of days per month with $UI_{ET} > 16$ m³ s⁻¹ km⁻¹ averaged from 1967 to 2008 along the western (42.5°N, 39.5°N) and northern (8.5°W, 5.5°W) coast of the IP. (b) Probability of finding consecutive days under upwelling favorable conditions ($UI_{ET} > 16$ m³ s⁻¹ km⁻¹) from 1967 to 2008 between April and September along the western coast of the IP (42.5°N, 39.5°N) and between June and August along the northern one (8.5°W, 5.5°W).

4. Discussion

Over the last decades several works were carried out in terms of upwelling along the northwestern coast of the Iberian Peninsula which have improved significantly the knowledge of this process. Nevertheless, most of these studies were mainly focused on the western or northern coast of the IP separately and therefore have different databases and temporal scales, making the comparison between both coasts more difficult. Thus, in order to do a more complete comparative analysis between the western and northern coast, upwelling conditions were analyzed over the last 42 years (1967–2008) in terms of upwelling indices calculated from Ekman transport data.

The UI_{ET} analysis showed the existence of inter-annual variability at the western and northern coast (Fig. 2(a–d)) with both patterns macroscopically similar showing maximum values in spring–summer and minimum ones in autumn–winter. In fact, the correlation coefficient calculated between both variables reached values of 0.6 ($p < 0.01$). Taking into account the mean annual evolution of UI_{ET} (Fig. 4(a–d)) it was observed that the season under more upwelling favorable conditions corresponds to spring–summer (April–September) along the western coast and only to summer (June–August) along the northern one. Nevertheless, the maximum value of UI_{ET} was observed in July at both coasts with higher values along the western coast (700 m³ s⁻¹ km⁻¹) than along the northern one (300 m³ s⁻¹ km⁻¹).

The behavior observed along the western coast agrees with the results found by the previous works carried out in this region (Alvarez et al., 2008b) showing that upwelling is a frequent phenomenon during the spring–summer months characterized by
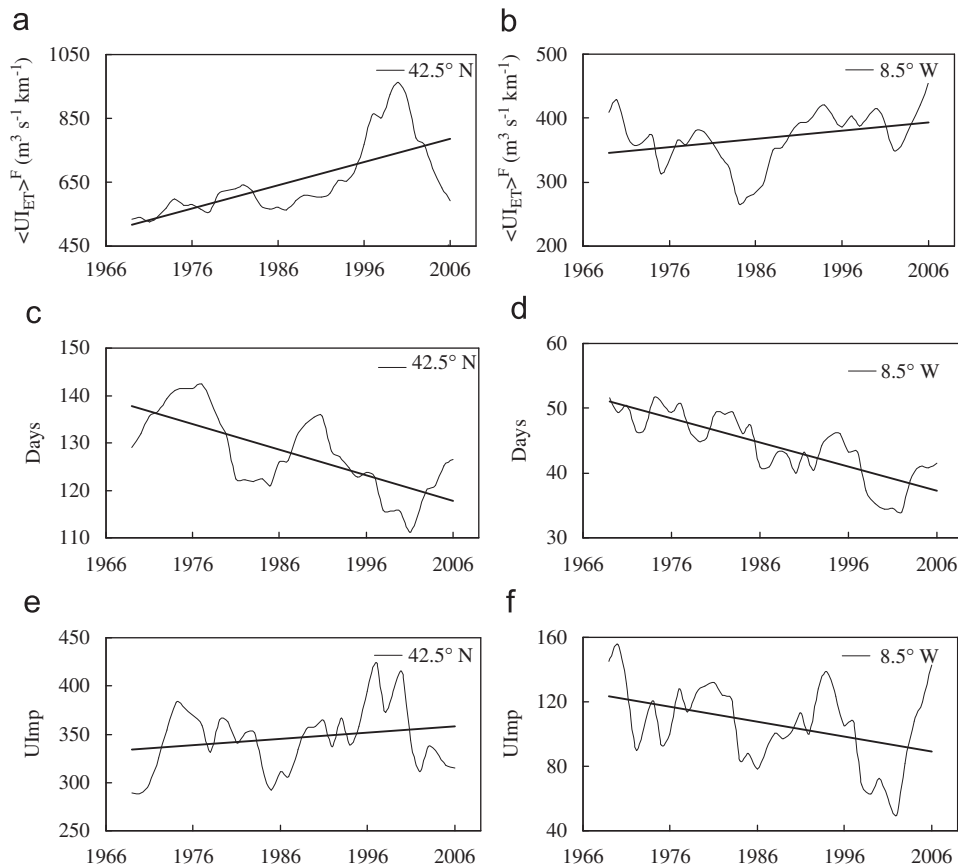

Fig. 7. Annual upwelling intensity averaged from April to September (1967–2008) at the western coast (a) and from June to August (1967–2008) at the northern coast (b). Number of days per year under upwelling favorable conditions averaged from April to September (1967–2008) at the western coast (c) and from June to August (1967–2008) at the northern one (d). U_{Imp} calculated at the western (e) and northern (f) coast. Straight lines in each frame show the linear fit at the control points ($p > 0.01$).

favorable northerly winds blowing along the shelf. In fact, from the analysis of the number of days under upwelling favorable conditions it was found that during this period, approximately 20–28 days per month kept these favorable conditions (Fig. 6(a)). It is also necessary to take into account that during autumn–winter the number of days under favorable conditions was not negligible (12–14 days per month) showing the possibility of observing upwelling events during this period (Santos et al., 2001, 2004; Alvarez et al., 2003; Borges et al., 2003; deCastro et al., 2006, 2008a; Prego et al., 2007). Thus, upwelling events should be observed under favorable conditions independently of the season. These results can also be compared with the situation observed by Cabanas and Alvarez (2005) and deCastro et al. (2008a), using Ekman transport data at the ocean (point 43°N, 11°W) for a 40-year period (1966–2005). On the one hand, the highest

number of days under upwelling favorable conditions obtained at the ocean point was also observed during the summer months (22–25 days per month). On the other hand, during the winter period it was also possible to observe a number of days under favorable conditions at this point (11–18 days per month) lower than along the western coast.

The situation corresponding to the northern coast (Fig. 6(a)) was similar to the one observed at the western one. The number of days under upwelling favorable conditions was higher during spring–summer (12–14 days month) than during autumn–winter (8–10 days per month) showing that upwelling events during this last period can also occur (Alvarez et al., 2009). Nevertheless, this number of days was lower than along the western coast throughout the year indicating that upwelling process is more frequent along the western coast. In fact, the probability of finding consecutive days under these favorable conditions (Fig. 6(b)) was also higher along the western coast. The highest probability values were observed between 1 and 5 consecutive days at both coasts with values decreasing from around 80% to 60% at the western coast and from around 50% to 20% at the northern one. This situation can be explained by the coastal orientation which modulates wind direction and intensity changing the upwelling favorable conditions prevalence at each coastal region (Torres et al., 2003; Gomez-Gesteira et al., 2006; Alvarez et al., 2008a). Possibly, this is the reason why upwelling research has been mainly focused on the western coast (Fraga, 1981; Alvarez-Salgado et al., 2000; Alvarez et al., 2005, 2008b).

Upwelling trends were also analyzed during the most upwelling favorable period along the western (April–September) and

Table 2
Trends of the mean $\langle UI_{ET} \rangle^F$, number of days and upwelling impact under favorable conditions ($UI > 16\, m^3\, s^{-1}\, km^{-1}$) corresponding to the period 1967–2008 at the western and northern coast of the Iberian Peninsula ($p < 0.01$).

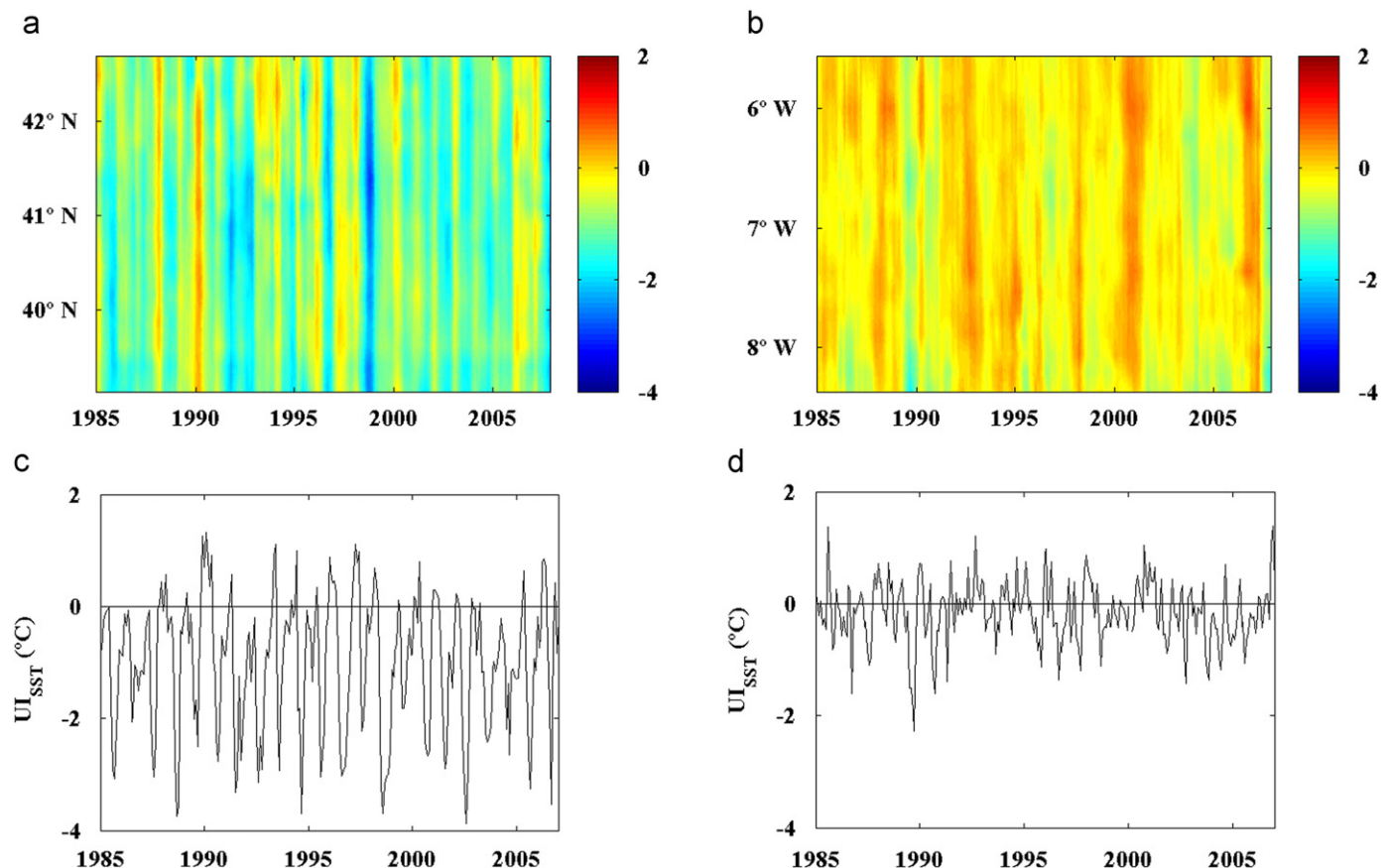|	$\langle UI_{ET} \rangle^F$	Days	UI_{Imp}
42.5°N	5	−0.4	0.4
41.5°N	6	−0.5	0.1
40.5°N	5	−0.5	0.2
39.5°N	3	−0.3	0.2
8.5°W	1	−0.4	−1
7.5°W	0.1	−0.3	−0.8
6.5°W	−0.2	−0.3	−1
5.5°W	−0.8	−0.2	−0.8

Fig. 8. Inter-annual evolution of UI_{SST} from 1967 to 2008 along the western (a) and northern (b) coast of the IP. Inter-annual evolution of the spatially averaged UI_{SST} from 1967 to 2008 along the western (c) and northern (d) coast of the IP.
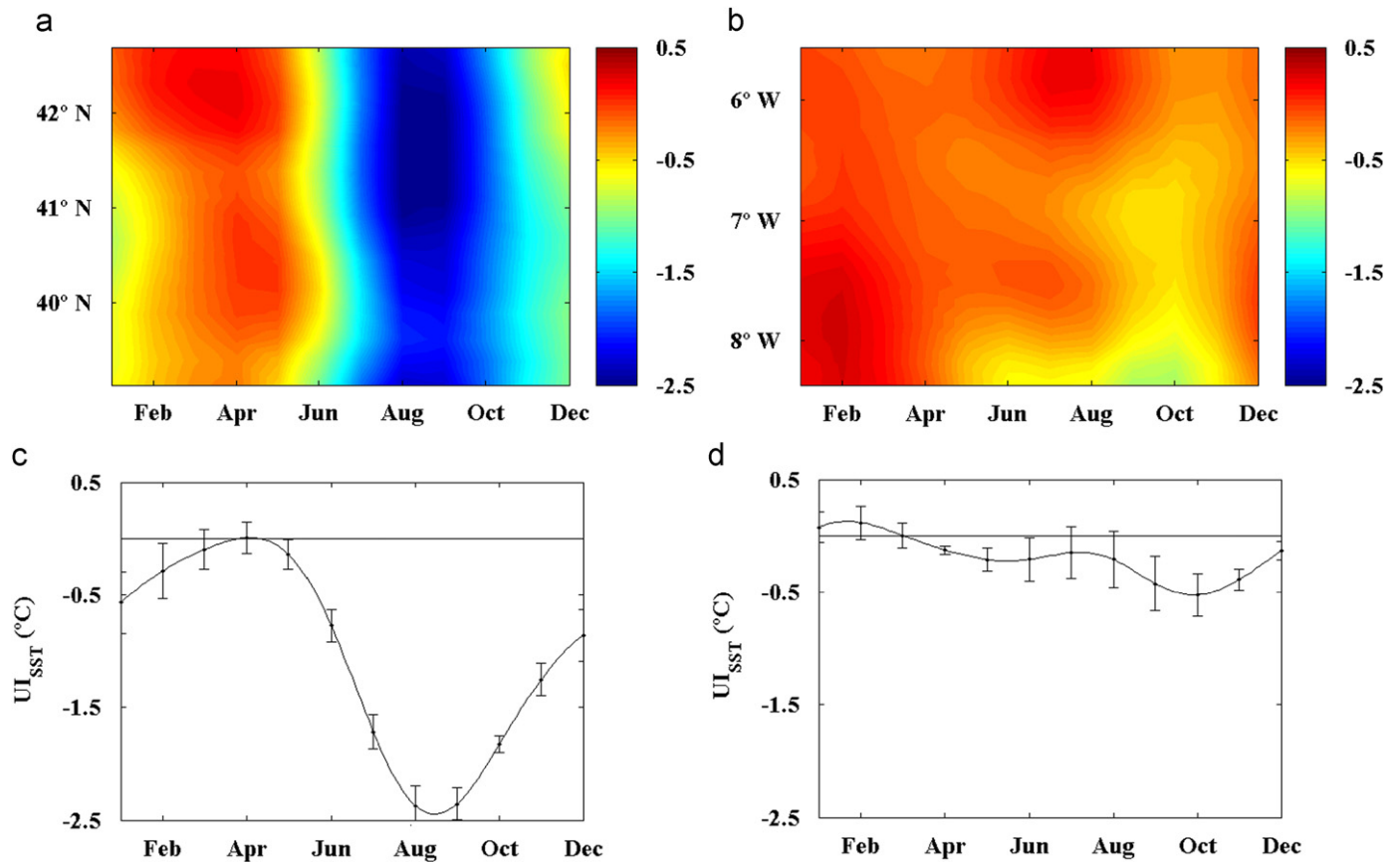
Fig. 9. Mean annual evolution of UI_{SST} from 1985 to 2008 along the western (a) and northern (b) coast of the IP. Annual cycle of UI_{SST} spatially averaged from 1985 to 2008 along the western (c) and northern (d) coast of the IP. Negative (positive) UI_{SST} values mean upwelling favorable (unfavorable) conditions.

northern (June–August) coast (Fig. 7(a–f), Table 2). Although previous studies have found that upwelling favorable winds have weakened from 1940s onward at the western (Lemos and Sanso, 2006; Alvarez-Salgado et al., 2008; Otero et al., 2008; Bode et al., 2009) and northern (Llope et al., 2006; Valdés et al., 2007) coast of the IP, from this analysis it was not observed a clear seasonal trend in UI obtaining confidence level values lower than 90%. Nevertheless, it was possible to see that the control points located along the western coast showed a relatively similar behavior, while along the northern one the control points presented a different pattern, which can be better observed taking into account the mean intensity of UI_{ET} (Table 2 $\langle UI_{ET} \rangle^F$). Along the western coast $\langle UI_{ET} \rangle^F$ showed positive values at all points while along the northern one positive values were observed at the 2 westernmost points and negative values at the 2 easternmost points. In fact, the correlation coefficient calculated for the 3 variables analyzed in Fig. 7 between the two control points located at the extreme part of each side of the IP coast reached values of 0.8 for the mean intensity of UI_{ET} along the western coast and 0.6 along the northern one. The variation in the number of days under upwelling favorable conditions also showed a higher correlation coefficient at the western coast (0.9) than at the northern one (0.6) and finally, the value of the correlation coefficient for the U_{Imp} was around 0.7 at both coasts.

The effect of the wind forcing on ocean water was analyzed in terms of SST differences which allow identifying the presence of upwelled water. Thus, the UI_{SST} was calculated at both coasts of the IP taking into account the temperature difference between coastal and oceanic points. The inter-annual evolution of the UI_{SST} (Fig. 8) showed differences among years at both coasts with

maximum values in autumn–winter and minimum ones (upwelling favorable conditions) in spring–summer. From the annual cycle (Fig. 9) it was found a clear upwelling season between June and November along the western coast with the strongest negative values observed in August–September. Taking into account the results corresponding to Fig. 4, the most upwelling favorable conditions from Ekman transport data can be observed in July showing the existence of a lag (1–2 months) between UI_{ET} and UI_{SST}. This lag has also been observed in previous studies (Fiuza et al., 1982; Nykjaer and Van Camp, 1994; deCastro et al., 2008b). At the northern coast the pattern is similar, although UI_{SST} minimum values were observed in September–October. In addition, from June to August UI_{SST} values showed a small increase with regard to the previous and the next months which was not observed at the western coast. This situation can be explained due to the SST warming which is observed in spring–summer at the south-eastern corner of the Bay of Biscay (Pingree and Le Cann, 1989; Koutsikopoulos and Le Cann, 1996; Gomez-Gesteira et al., 2008), which can increase the temperature values at the coastal points considered along the northern coast.

Chlorophyll concentrations were also analyzed along both coasts in order to characterize the implications of upwelling for the ecosystem. At the western coast (Fig. 10(a, c)) chlorophyll showed a high seasonal variability with the highest concentrations values in spring–summer months. The chlorophyll pattern observed at the Corcubion Sound agrees with the situation analyzed by Varela et al. (2010) at the same region. In addition, the results obtained at both control points coincide with those observed by Bode et al. (2009) considering data from 1989 to 2006 in a control station located in front of the western Galician
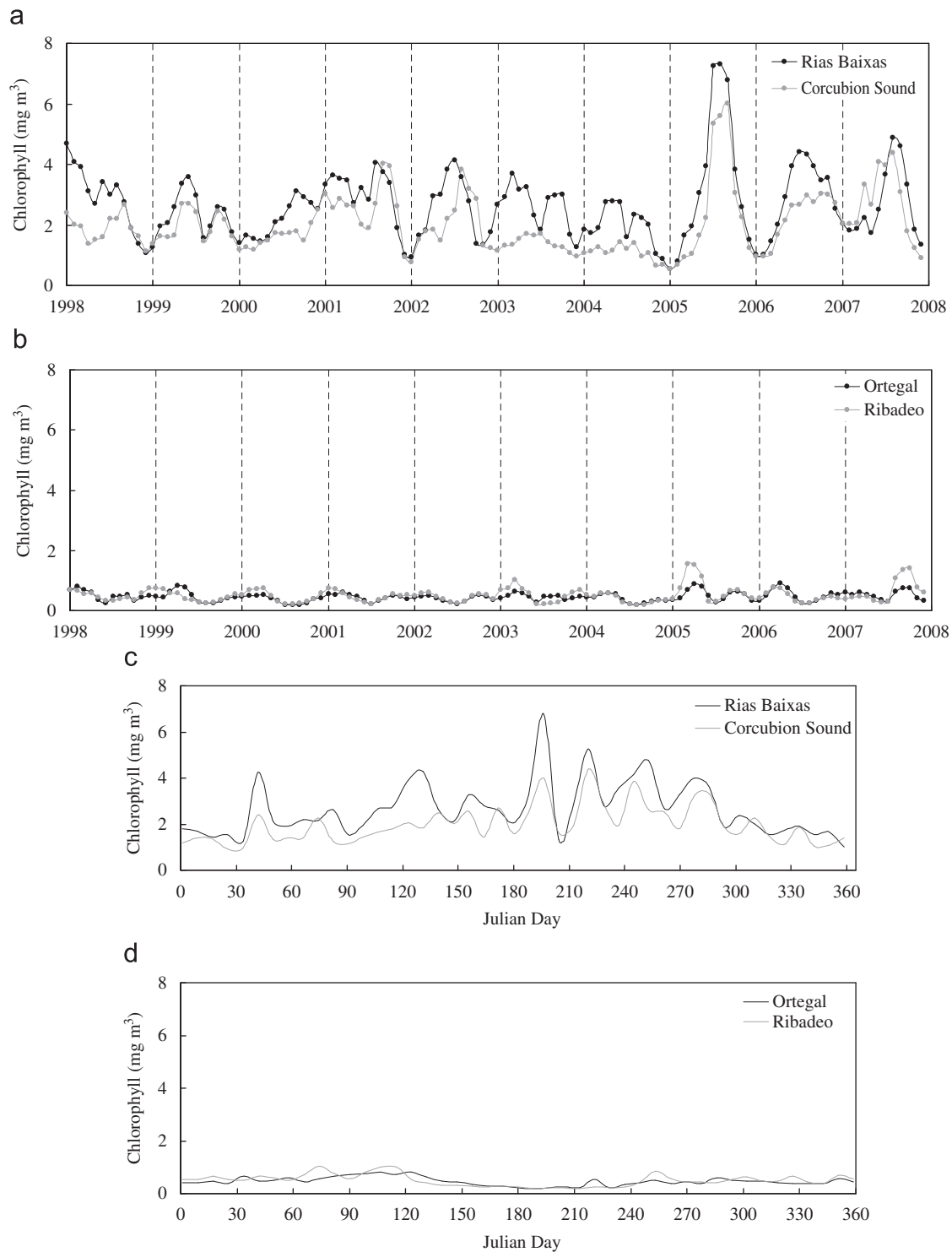
Fig. 10. Inter-annual evolution of chlorophyll concentration from 1998 to 2007 along the western (a) and northern (b) coast of the IP. Mean annual cycle of chlorophyll concentration from 1998 to 2007 along the western (c) and northern (d) coast of the IP.

coast. These authors found that from 1991 to 1995 chlorophyll blooms concentrated between spring and autumn. Nevertheless, in recent years blooms occurring in the summer increased relative to those in early spring or autumn. At the northern coast (Fig. 10(b, d)) the variation of chlorophyll concentrations was lower than along the western coast showing the maximum values in spring and autumn months and the minimum ones in summer months. This situation is characteristic of the typical planktonic cycle along the Cantabrian coast: a winter mixing period followed

by a summer stratification period, and phytoplankton blooms developing in the transition periods, mixing-stratification (spring bloom) and stratification-mixing (autumn bloom) (Varela et al., 2001, 2005, 2008, 2010). The difference between both coasts could be explained by the occurrence of summer upwelling events, which are more frequent along the western coast (Figs. 4 and 9). These summer upwelling events are related to the presence of ENACW (Fiuza, 1984; Ríos et al., 1992) near coast, which can be upwelled inside the estuaries located along this

region. The upwelling of ENACW fertilizes coastal waters generating a primary production which is important for fisheries and aquaculture in the area justifying that most of the studies carried out in terms of summer upwelling were focused in this coast. Eastward of Cape Ortegal ENACW is also present although upwelling is not a common event (Figs. 4 and 9). This water mass also fertilizes surface waters resulting in a primary production increase (Fernandez and Bode, 1991; Llope et al., 2006) although these phytoplankton productive events are less important than those observed south of Cape Finisterre (Varela et al., 2005).

5. Summary and conclusions

The upwelling influence along the northwestern coast of the Iberian Peninsula has been characterized by a comparative analysis between the western and northern coast. The analysis was carried out in terms of wind-induced upwelling and water response to this forcing. The results obtained from this comparative analysis have shown the following:

(1) The temporal evolution of the UI_{ET} showed a similar annual cycle at both coasts, although the season under more upwelling favorable conditions was observed from April to September along the western coast and from June to August along the northern one with the maximum value of UI_{ET} in July at both coasts.

(2) Considering the upwelling season common to both coasts (June–August), it was found that the most probable situation corresponded to upwelling favorable conditions along both coasts ($\sim$46%) followed by upwelling unfavorable conditions also along both coasts ($\sim$26%). In addition, inter-decadal variations were observed.

(3) The highest number of days per month under upwelling favorable conditions was observed during the upwelling season at both coasts with higher values along the western coast (20–28 days) than along the northern one (12–14 days). In addition, the probability of finding consecutive days under these favorable conditions was also higher along the western coast

(4) A clear seasonal trend was not observed from the analysis of the number of days under upwelling favorable conditions and the upwelling intensity during these days (upwelling impact) (confidence level lower than 90%).

(5) SST analysis also showed the existence of a clear upwelling season along both coasts with a pattern of UI_{SST} similar to the one corresponding to UI_{ET}. Nevertheless, the strongest upwelling favorable conditions have 1–2 months lag with respect to the maximum UI_{ET}.

(6) At the western coast chlorophyll concentrations showed a high seasonal variability with the highest concentrations values in spring–summer months while at the northern coast the maximum values were observed in spring and autumn and the minimum ones in summer.

Acknowledgements

References

Alvarez, I., deCastro, M., Prego, R., Gomez-Gesteira, M., 2003. Hydrographic characterization of a winter-upwelling event in the Ria of Pontevedra (NW Spain). Estuarine Coastal and Shelf Science 56, 869–876.

Alvarez, I., deCastro, M., Gomez-Gesteira, M., Prego, R., 2005. Inter- and intra-annual analysis of the salinity and temperature evolution in the Galician Rías Baixas–ocean boundary (northwest Spain). Journal of Geophysical Research 110, C04008. doi:10.1029/2004JC002504.

Alvarez, I., Gomez-Gesteira, M., deCastro, M., Novoa, E.M., 2008a. Ekman Transport along the Galician Coast (NW, Spain) calculated from QuikSCAT winds. Journal of Marine Systems 72, 101–115.

Alvarez, I., Gomez-Gesteira, M., deCastro, M., Dias, J.M., 2008b. Spatio-temporal evoltion of upwelling regime along the western coast of the Iberian Península. Journal of Geophysical Research 113, C07020. doi:10.1029/2008JC004744.

Alvarez, I., Ospina-Alvarez, N., Pazos, Y., deCastro, M., Bernardez, P., Campor, M.J., Gomez-Gesteira, J.L., Alvarez-Ossorio, M.T., Varela, M., Gomez-Gesteira, M., Prego, R., 2009. A winter upwelling event in the Northern Galician Rias: frequency and oceanographic implications. Estuarine Coastal and Shelf Science 82, 573–582. doi:10.1016/j.ecss.2009.02.023.

Alvarez, I., Gomez-Gesteira, M., deCastro, M., Gomez-Gesteira, J.L., Dias, J.M., 2010. Summer upwelling frequency along the western Cantabrian coast form 1967 to 2008. Journal of Marine Systems 79, 218–226.

Alvarez- Salgado, X.A., Gago, J., Miguez, B.M., Gilcoto, M., Perez, F.F., 2000. Surface waters of the NW Iberian Margin: upwelling on the shelf versus outwelling of upwelled waters from the Rias Baixas. Estuarine Coastal and Shelf Science 51, 821–837.

Alvarez- Salgado, X.A., Nieto-Cid, M., Gago, Brea, S., Castro, C.G., Doval, M.D., Perez, F.F., 2006. Stoichiometry of the degradation of dissolved and particulate biogenic organic matter in the NW Iberian upwelling. Journal of Geophysical Research 111 (C07017). doi:10.1029/2004JC002473.

Alvarez-Salgado, X.A., Labarta, U., Fernández-Reiríz, M.J., Figueiras, F.G., Rosón, G., Piedracoba, S., Filgueira, R., Cabanas, J.M., 2008. Renewal time and the impact of harmful algal blooms on the extensive mussel raft culture of the Iberian coastal upwelling system. Harmful Algae 7, 849–855. doi:10.1016/j.hal.2008.04.007.

Bakun, A., 1973. Coastal Upwelling Indexes, west coast of North America, 1946–71. NOAA Technical Report NMF, 671, p. 103.

Bode, A., Varela, M., Casas, B., Gonzalez, N., 2002. Intrusions of eastern North Atlantic central waters and phytoplankton in the north and northwestern Iberian shelf during spring. Journal of Marine Systems 36, 197–218.

Bode, A., Alvarez-Ossorio, M.T., Cabanas, J.M., Miranda, A., Varela, M., 2009. Recent trends in plankton and upwelling intensity off Galicia (NW Spain). Progress in Oceanography 83, 342–350.

Borges, M.F., Santos, A.M.P., Crato, N., Mendes, H., Mota, B., 2003. Sardine Regime shifts off Portugal: a time series analysis of catches and wind conditions. Scientia Marina 67, 235–244.

Botas, J., Fernandez, E., Bode, A., Anadon, R., 1990. A persistent upwelling off the Central Cantabrian Coast (Bay of Biscay). Estuarine Coastal and Shelf Science 30, 185–199.

Borja, A., Uriarte, A., Valencia, V., Motos, L., Uriarte, A., 1996. Relationships between anchovy (*Engraulis encrasicholus*) recruitment and the environment in the Bay of Biscay. Scientia Marina 60, 179–192.

Borja, A., Fontan, A., Saenz, J., Valencia, V., 2008. Climate, oceanography and recruitment: the case of the Bay of Biscay anchovy (*Engraulis encrasicolus*). Fisheries Oceanography 17, 477–493.

Cabanas, J.M., Alvarez, I., 2005. Ekman transport patterns in the area close to the Galician coast (NW, Spain). Journal of Atmospheric and Oceanographic Science 10, 325–341.

deCastro, M., Dale, A.W., Gomez-Gesteira, M., Prego, R., Alvarez, I., 2006. Hydrographic and atmospheric analysis of an autumnal upwelling event in the Ria of Vigo (NW Iberian Peninsula). Estuarine Coastal and Shelf Science 68, 529–537. doi:10.1016/j.ecss.2006.03.004.

deCastro, M., Gomez-Gesteira, M., Alvarez, I., Cabanas, J.M., Prego, R., 2008a. Characterization of fall-winter upwelling recurrence along the Galician western coast (NW Spain) from 2000 to 2005: dependence on atmospheric forcing. Journal of Marine Systems 72, 145–148. doi:10.1016/j.jmarsys.2007.04.005.

deCastro, M., Gomez-Gesteira, M., Lorenzo, M.N., Alvarez, I., Crespo, A.J.C., 2008b. Influence of atmospheric modes on coastal upwelling along the western coast of the Iberian Peninsula, 1985 to 2005. Climate Research 36, 169–179. doi:10.3354/cr00742.

Fernandez, E., Bode, A., 1991. Seasonal patterns of primary production in the Central Cantabrian Sea (Bay of Biscay). Scientia Marina 55, 629–636.

Fiuza, A.F.G., 1984. Hidrologia e dinâmica das águas costeiras de Portugal (Hydrology and dynamics of the Portuguese coastal water). Ph.D. Dissertation, University of Lisboa, Lisboa, 294 pp.

Fiuza, A., Macedo, M.E., Guerreiro, M.R., 1982. Climatological space and time variation of the Portuguese coastal upwelling. Oceanologica Acta 5, 31–40.

Fontan, A., Valencia, V., Borja, A., Goikoetxea, N., 2008. Oceano-meteorological conditions and coupling in the southeastern Bay of Biscay, for the period

2001–2005: a comparison with the past two decades. Journal of Marine Systems 72, 167–177.

Fraga, F., 1981. Upwelling off the Galician Coast, Northwest Spain. In: Richardson, F.A. (Ed.), Coastal Upwelling. American Geophysical Union, Washington, pp. 176–182.

Frouin, R., Fiuza, A.F.G., Ambar, I., Boyd, T.J., 1990. Observations of a poleward surface current off the coasts of Portugal and Spain during winter. Journal of Geophysical Research 95, 679–691.

Garcia-Soto, C., Pingree, R.D., Valdes, L., 2002. Navidad development in the southern Bay of Biscay: climate change and swoddy structure from remote sensing and in situ measurements. Journal of Geophysical Research, 107. doi:10.1029/2001JC001012.

Gomez-Gesteira, M., Moreira, C., Alvarez, I., deCastro, M., 2006. Ekman transport along the Galician coast (NW, Spain) calculated from forecasted winds. Journal of Geophysical Research 111, C10005. doi:10.1029/2005JC003331.

Gomez-Gesteira, M., deCastro, M., Alvarez, I., Gomez-Gesteira, J.L., 2008. Coastal sea surface temperature warming trend along the continental part of the Atlantic Arc (1985–2005). Journal of Geophysical Research 113, C04010. doi:10.1029/2007JC004315.

Koutsikopoulos, C., Le Cann, B., 1996. Physical processes and hydrological structures related to the Bay of Biscay anchovy. Scientia Marina 60, 9–19.

Lavin, A., Valdes, L., Gil, J., Moral, M., 1998. Seasonal and inter-annual variability in properties of surface water off Santander, Bay of Biscay, 1991–1995. Oceanologica Acta 21, 179–190.

Lemos, R.T., Sanso, B., 2006. Spatio-temporal variability of ocean temperature in the Portugal Current System. Journal of Geophysical Research, 111. doi:10.1029/2005JC003051.

Llope, M., Anadon, R., Viesca, L., Quevedo, M., Gonzalez-Quiros, R., Stenseth, N.C., 2006. Hydrography of the southern Bay of Biscay shelf-break region: integrating the multiscale physical variability over the period 1993–2003. Journal of Geophysical Research 111, C09021. doi:10.1029/2005JC002963.

Nykjaer, L., Van Camp, L., 1994. Seasonal and Interannual variability of coastal upwelling along northwest Africa and Portugal from 1981 to 1991. Journal of Geophysical Research 99 (C7), 14197–14207.

Otero, J., Álvarez-Salgado, X.A., González, Á.F., Miranda, A., Groom, S.B., Cabanas, J.M., Casas, G., Wheatley, B., Guerra, Á., 2008. Bottom-up control of common octopus Octopus vulgaris in the Galician upwelling system, northeast Atlantic Ocean. Marine Ecology Progress Series 362, 181–192.

Pingree, R.D., Le Cann, B., 1989. Celtic and Armorican slope and shelf residual currents. Continental Shelf Research 23, 303–338.

Prego, R., Guzmán-Zuñiga, D., Varela, M., deCastro, M., Gomez-Gesteira, M., 2007. Consequences of winter upwelling events on biogeochemical and phytoplankton patterns in a western Galician ria (NW Iberian Peninsula). Estuarine Coastal and Shelf Science 73, 409–422.

Ríos, A.F., Pérez, F.F., Alvarez-Salgado, X.A., Figueiras, F.G., 1992. Water masses in the upper and middle North Atlantic Ocean east of the Azores. Deep-Sea Research 39, 645–658.

Santos, A.M., Borges, M.F., Groom, S., 2001. Sardine and horse mackerel recruitment and upwelling off Portugal. ICES Journal of Marine Science 58, 589–596.

Santos, A.M.P., Peliz, A., Dubert, J., Oliveira, P.B., Angelico, M.M., Re, R., 2004. Impact of a winter upwelling event on the distribution and transport of sardine (Sardina pilchardus) eggs and larvae off western Iberia: a retention mechanism. Continental Shelf Research 24, 149–165.

Santos, A.M., Kazmin, A.S., Peliz, A., 2005. Decadal changes in the Canary upwelling system as revealed by satellite observations: their impact on productivity. Journal of Marine Research 63, 359–379.

Torres, R., Barton, E.D., Miller, P., Fanjul, E., 2003. Spatial patterns of wind and sea surface temperature in the Galician upwelling region. Journal of Geophysical Research 108, 3130–3143. doi:10.1029/2002JC001361.

Valdés, L., López-Urrutia, A., Cabal, J., Alvarez-Ossorio, M., Bode, A., Miranda, A., Cabanas, M., Huskin, I., Anadón, R., Alvarez-Marqués, F., Llope, M., Rodríguez, N., 2007. A decade of sampling in the Bay of Biscay: what are the zooplankton time series telling us? Progress in Oceanography 74 98–114.

Varela, M., Prego, R., Belzunce, M.J., Martín-Salas, F., 2001. Inshore–offshore differences in seasonal variations of phytoplankton assemblages: the case of a Galician Ria Alta (A Coruña Ria) and its adjacent shelf (NWSpain). Continental Shelf Research 21, 1815–1838.

Varela, M., Prego, R., Pazos, Y., Moroño, A., 2005. Influence of upwelling and river runoff interaction on phytoplankton assemblages in a Middle Galician Ria and comparison with northern and southern rias (NW Iberian Peninsula). Estuarine Coastal and Shelf Science 64, 721–737.

Varela, M., Prego, R., Pazos, Y., 2008. Spatial and temporal variability of phytoplankton biomass, primary production and community structure in the Pontevedra Ria (NW Iberian Peninsula): oceanographic periods and possible response to environmental changes. Marine Biology 154, 483–499.

Varela, M., Alvarez-Ossorio, M., Bode, A., Prego, R., Bernardez, P., Garcia-Soto, C., 2010. The effects of a winter upwelling on biogeochemical and planktonic components in an area close to the Galician upwelling core: the Sound of Corcubion (NW Spain). Journal of Sea Research 64, 260–272.